Optimisation of flywheel energy storage systems with geared transmission for hybrid vehicles

M G Read[1], R A Smith[2], K R Pullen[3]

[1] Imperial College London, South Kensington Campus, London SW7 2AZ
Corresponding author; Email: m.read@city.ac.uk, Tel: +44 20 7040 8795
(Present address; City University London, Northampton Square, London EC1V 0HB, UK)

[2] Imperial College London, South Kensington Campus, London SW7 2AZ, UK

[3] City University London, Northampton Square, London EC1V 0HB, UK

Keywords

Flywheel; hybrid; continuously variable transmission; regenerative braking; energy storage; optimisation

Abstract

Flywheel energy storage devices may be coupled to mechanical transmissions for braking energy recovery and the provision of additional power for acceleration in hybrid vehicles. Power transmission across a continuous range of speed ratios is necessary. The flywheel size and depth-of-discharge must be chosen for a particular application, and this has a direct effect on transmission efficiency, required gearing ratios and mass of components. Optimisation of these parameters requires a fundamental understanding of this interaction, which has not previously been investigated and reported. To address this, the current paper presents a new method of analysing mechanical flywheel systems. A simple algebraic analysis can be used to specify flywheel system parameters for any regenerative braking application where the flywheel is used to provide initial acceleration of the vehicle from stationary. This has been applied to systems using geared transmissions with continuous speed variation achieved though sliding contact in clutch and brake components. The results of the analysis highlight how the optimum selection of flywheel depth-of-discharge must achieve a balance between high transmission efficiency and low system mass. This is illustrated for a passenger car application, allowing a full assessment of system performance and the specification of appropriate design parameters.

Abbreviations

CGB = Control Gear Box
CST = Continuous Slip Transmission
CVT = Continuously Variable Transmission
DDC = Dual Differential Coupled
FDC = Final Drive Coupled
PGS = Planetary Gear Set

Nomenclature

$\bar{E}$ = specific energy capacity
$\bar{T}$ = specific torque capacity
E = energy
G_j = general fixed gear ratio in CGB (where j has a value between 1 and N_{cgb})
J = moment of inertia
K = fixed gear ratio connecting to CGB to PGS or vehicle final drive
m = mass
N = total number of PGSs in a transmission
N_{cgb} = number of fixed gear ratios in CGB
P = power
R_n = characteristic gear ratio of a general PGS in a multi-PGS brake controlled transmission (where n has a value between 1 and N)
R_p and R_q = characteristic gear ratio of general PGSs in a CGB controlled transmission

r_w = vehicle wheel radius
T = torque
v = velocity

η_n, η_p, η_q = efficiency of the corresponding general PGS
η_{trans} = instantaneous transmission efficiency
$\bar{\eta}$ = mean transmission efficiency
λ = flywheel depth-of-discharge
ω = angular velocity

SUBSCRIPTS

ch = relating to flywheel charging operation
cyc = relating to the charge-discharge cycle
dis = relating to flywheel discharge operation
f = final
fd = relating to final drive of vehicle
fw = relating to flywheel
i = initial
sys = relating to the total flywheel system
veh = relating to the vehicle

1. Background

Flywheel energy storage systems with mechanical transmissions allow regenerative braking and power augmentation during acceleration in automotive vehicles. The development of this technology is being driven by rising fuel costs and tightening emissions legislation. In recent years the issue of climate change has generated great scientific and public interest in the effect of human activity on the environment. The production of greenhouse gasses has been linked with global temperature rises [1], and in the light of reports such as the Stern Review on the economic impact of climate change [2] a general consensus appears to have been reached on the need to limit such emissions. Road vehicles account for a significant proportion of the total world energy use and energy-related CO_2 emissions, and stabilisation of atmospheric CO_2 concentrations is likely to require continuous improvements in vehicle efficiency over the next 40 years as mapped out by the IEA [3].

Many fuel saving technologies are currently available, but the associated increase in vehicle cost appears to be limiting widespread implementation. Power-train hybridisation is an attractive option for achieving significant fuel savings, especially when combined with other energy saving measures such as stop-start engine operation. However, even a simple mild hybrid system can add around 20% [3] to the cost of a typical passenger car, largely due to the high cost of electric motors and electrochemical batteries relative to conventional powertrain components. Several types of energy storage device are available for use in hybrid vehicles, and an initial indication of their suitability can be obtained from the Ragone plot [4], which show the specific energy and specific power that can be achieved with different energy storage technologies. The more detailed analysis presented by Stewart et al. [5] shows how lithium-ion batteries and supercapacitors can be optimised for hybrid electric vehicle applications, where a discharge time of 10s has been assumed. Ceraolo et al. [6] obtained similar results, but state that the power limitation of lithium-ion batteries occurs during charging where the current must be limited to avoid damage; for effective regenerative braking with a charging period of 10s, the specific power was found to be only 16% of that achieved for charging over the same period. In this case, the battery had a measured specific power (excluding packaging weight) of 330 W/kg, and charge-discharge efficiency of 85%, while the supercapacitor achieved around 720 W/kg and 87% respectively. The corresponding specific energy of these devices is in the region of 15-30 kJ/kg for the hybrid vehicle application [5]. It is important to note that the efficiency values do not include the additional losses that would occur in the electric motor and associated power control electronics of a vehicle during charge and discharge, and that the mass of these additional components and packaging will significantly reduce the specific power and specific energy of the system. There are also limitations to battery cycle life and difficulties with recycling the expensive materials used in modern high performance batteries. In recent years, flywheels have received considerable attention as an alternative to electrical energy storage that can potentially offer low cost and long operational life, and are discussed in more detail in the following section. In summary, it is clear that there is a compromise between improving specific fuel consumption and increasing the total cost of the vehicle which is highly dependent on the type of hybrid system and energy storage device used.

2. Hybrid technologies

Hybrid vehicles are defined as having more than one power source. The most common hybrid configurations consist of a primary power source, such as an internal combustion engine (ICE), combined with an energy storage device. This storage device must be capable of;

i) Accepting power from the vehicle during braking and/or from the primary power source,

ii) Delivering power to the vehicle for traction and/or auxiliary power loads.

Hybrid vehicles can be classified by the degree to which these conditions are satisfied; from micro and mild hybrids with limited energy capacity and operating flexibility, to full hybrids and electric vehicles. A sub-classification of full hybrid vehicles as either parallel or series can be made according to the configuration of the transmission connecting the primary power source and energy storage device to the final drive of the vehicle. The choice of transmission configuration is dependent on the aims of the hybridisation strategy and the nature of the energy storage device.

Advanced flywheels fabricated from composite materials have been shown to combine high specific energy and specific power, making them suitable for automotive regenerative braking applications where the typical charging time is of the order of 10 seconds [7-11]. Such flywheels are passive devices requiring an actively controlled transmission that is capable of applying torque to the flywheel in order to achieve discharge and recharge of the device. Mechanical and electrical transmissions can be used, and achieve similar overall efficiency. While flywheels with electrical transmissions can allow more flexible power train operation, mechanical transmissions are potentially cheaper and easier to integrate with conventional vehicle systems.

2.1. Mechanical flywheel systems

Continuously variable transmissions (CVTs) are required to achieve the continuous range of output-to-input speed ratios necessary for flywheel energy storage systems. This can be achieved using mechanisms such as toroidal [12] and push-belt [13] drives. Their use is limited by the range of gear ratios that can be spanned, but can be used directly to achieve flywheel systems such as in the commercialised system described by Brockbank [14, 15] and the systems analysed by Bottiglione et al. [16]. The use of CVTs in a power split configuration can increase the overall ratio range, but this increases the transmission complexity. A number of authors have discussed the concept of the power split CVT (PSCVT) [17-24], which have been considered as either lossless systems or as one directional systems, while Bottiglione and Mantriota [25] have investigated transmission efficiency for bi-directional flow in a PSCVT with a specific gear ratio spread. Several authors [14-16, 26-30] have investigated either direct CVTs or PSCVTs for flywheel applications. In these studies, the flywheel size and depth-of-discharge have been assigned fixed values, and the performance of particular transmission configurations has then been investigated, often in terms fuel consumption rather than performance of the flywheel system. No consideration has been given to the effect of depth-of-discharge on the transmission efficiency, required gear ratios and system mass, and no attempt has been made to optimise system parameters for particular applications. These issues are addressed in this paper through the use of a novel analysis method that allows the flywheel system parameters to be optimised. This is demonstrated using the specific energy of the flywheel system (i.e. the energy delivered to the vehicle during flywheel discharge per unit mass of the system) as a target function. This method provides a simple tool for specifying the component sizes and gearing ratios required for practical applications.

An alternative to the variator controlled transmissions described above is to use fixed ratio gearing with sliding contact in brake or clutch components. The use of clutches to achieve smooth and controlled power transfer in flywheel systems has been demonstrated by van Berkel et al. [31]. The current research describes two geared transmission architectures that achieve the continuous variation in speed ratio required for flywheel systems. The first is an extension of the brake-controlled planetary gear set (PGS) described by Diego-Ayala et al. [32] in which sequential use of multiple PGSs and optimisation of gear ratios achieves improved transmission efficiency. Secondly, a novel power split configuration using one or more PGSs is implemented, with power flow controlled by a conventional discrete ratio gear box and clutch. Both transmission types are referred to here as ‘continuous slip transmissions’ (CSTs), and are similar in principle to conventional automatic and dual clutch power-shift transmissions for ICEs. The large number of gear ratios used in these transmissions makes optimisation essential. An overview of the configuration and operation of these CSTs is presented in Section 3, and detailed analysis of flywheel systems using these transmissions is discussed in Section 4. Finally, Section 5 presents an example of how the normalised results of the flywheel system analysis can be used to identify the optimum system parameters for a particular application; in this case, a passenger car operating under typical urban driving conditions.

3. General discussion of continuous slip transmission architectures

The most basic type of continuous slip transmission consists of either a gear pair and clutch, or a PGS and brake. In both cases, power is transferred by applying a contact force between the slipping surfaces in the clutch or brake component. This creates an equal and opposite torque that can discharge or charge the flywheel while accelerating or decelerating the vehicle. Two examples of these transmission configurations are illustrated in Figure 1. The brake-controlled PGS transmission is discussed in detail in Section 4.

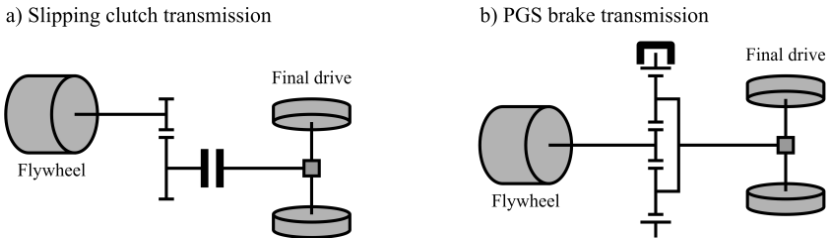

Figure 1 – Example of a) gear pair and clutch transmission and b) PGS and brake transmission (shown for a simple PGS with sun, carrier and ring branches connected to flywheel, vehicle and brake respectively)

For both transmissions shown in Figure 1, the ratio of vehicle to flywheel speed becomes constant when the slip-speed in the clutch or brake is zero. If the flywheel is used to accelerate the vehicle from stationary, this limits the depth-of-discharge, λ, of the flywheel, as defined in Equation 1.

$$\lambda = \frac{E_{fw,\max} - E_{fw,\min}}{E_{fw,\max}} = 1 - \left(\frac{\omega_{fw,\min}}{\omega_{fw,\max}} \right)^2 \tag{1}$$

The mean transmission efficiency of charging or discharging the flywheel is limited by the energy dissipated by the contact force at the slipping surfaces in either the clutch or brake. Increasing the number of discrete gear ratios in the CST, for example by using multiple PGSs as shown in Figure 2, allows the same ratio range to be covered with lower average slipping speed in the clutch/brake components. This results in less energy dissipation and increases mean transmission efficiency. There are however practical considerations that limit the number of gearing ratios in a conventional gearbox due to the increasing mass, complexity and cost of the system.

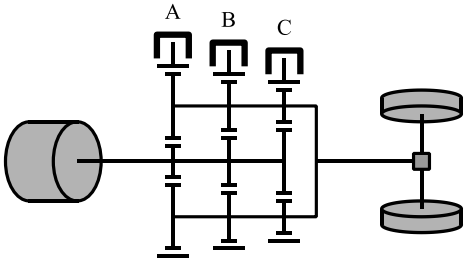

Figure 2 – Example of a multistage brake-controlled CST using 3 PGSs

Alternatively, combining gear pairs and PGSs in a power-split transmission allows the reuse of these gearing elements to achieve a large overall number of discrete gear ratios for the transmission. A power-split configuration is proposed in which a control gearbox (CGB) is connected to the 'control' branches of one or more PGSs, and provides a secondary path for power to flow between the vehicle and flywheel. An example of a continuous-slip power-split transmission consisting of two PGSs and a simple 4-speed countershaft gearbox (referred to as a 2-PGS, 4-CGB transmission) is illustrated in Figure 3. Various clutches are used to connect gearing for periods of operation, but power is only transmitted during sliding contact in the control clutch, c_s, or the PGS brakes. The operating sequence of this transmission for charge and discharge events is summarised in Table 1, and the operation is discussed in more detail in Section 4. It will be shown that no power recirculation occurs with this configuration, and that the reuse of gearing elements combined with the reduced power flow in many of the components offers the possibility of a compact and efficient transmission for flywheel applications.

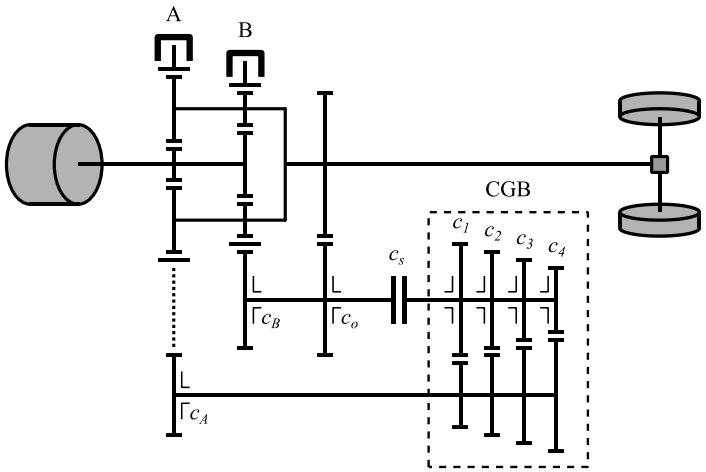

Figure 3 – Example of a CGB controlled transmission with 2 PGSs and a 4-speed CGB (dotted line represents an out-of-plane gear mesh)

Phase	***Connecting clutch***							***Control component***			***Description of operation***
	CGB gear clutch				Shaft clutch			PGS brake		Control clutch, c_s	
	c_1	c_2	c_3	c_4	c_o	c_A	c_B	A	B		
1	x				x	x				x	Clutch controlled power split between final drive and PGS A
2		x			x	x				x	
3			x		x	x				x	
4				x	x	x				x	
5								x			Brake controlled at PGS A
6				x		x	x			x	Clutch controlled power split between PGS A and PGS B
7			x			x	x			x	
8		x				x	x			x	
9	x					x	x			x	
10									x		Brake controlled at PGS B

Table 1 – Control sequence for 2-PGS, 4-speed CGB controlled transmission shown in Figure 3, where crosses indicate the transmission elements in use (sequence of phases is 1-10 for full discharge and 10-1 for full charge)

4. Analysis of flywheel systems

Full numerical optimisation of a hybrid powertrain using time-step based vehicle simulation requires detailed component models, and specific information about the vehicle and drive cycle, along with a realistic power control strategy. A comprehensive overview of suitable vehicle modelling and simulation techniques is provided by Guzzella and Sciarretta [33] which considers both quasi-static and dynamic modelling approaches. Dynamic system modelling can be implemented using a range of tools [34, 35] and is highly suited to vehicle power-train simulation. Using these numerical methods it is, however, computationally intensive to optimise parameters of the energy storage system (flywheel energy capacity, depth-of-discharge, component torque rating and multiple transmission gear ratios), particularly when the system contains a large number of variables. Previous studies have focussed on optimising the control of powertrains with fixed component parameters [36, 37]. In order to optimise these parameters, the approach presented here makes several assumptions that simplify and generalise the analysis of mechanical flywheel systems:

i. Lossless vehicle and flywheel models; the torque acting on these components is therefore proportional to the rate of change of angular speed, as shown in Equation 2.

$$T_{fd} = J_{fd}\frac{d\omega_{fd}}{dt}, \text{ and } T_{fw} = J_{fw}\frac{d\omega_{fw}}{dt} \quad (2)$$

ii. Constant efficiency gearing; this applies to both gear pairs and planetary gearing.

iii. Simple flywheel control strategy; the flywheel is used to provide all tractive power from vehicle launch until depleted (i.e. until the transmission is no longer able to discharge the flywheel).

By applying these assumptions, the operation of the flywheel system can be described algebraically. This allows simple multi-variable optimisation of the multiple system parameters, and provides a rigorous basis for comparing the performance of different system configurations. The results are normalised by the ratio of vehicle inertia to flywheel inertia, and so can be used to size gear ratios and components for any appropriate hybrid vehicle application. The most important component of the CSTs considered in this paper is the planetary gear set, which is described below.

4.1. Planetary gear set characteristics

The planetary gear set (PGS) is a key component in continuous slip transmissions. The gearing configurations used in two types of PGS are illustrated in Figure 4.

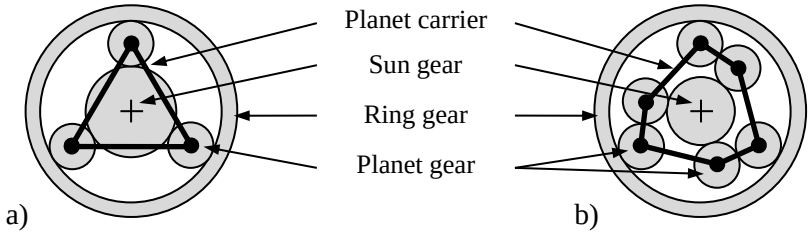

Figure 4 – Configuration of a) simple PGS and b) PGS with idler planet gears

When the sun, ring and planet-carrier branches are free to rotate, the PGS has 2 degrees of freedom, allowing either:

- Power input at a single branch to be split between 2 outputs, or,
- Power input at 2 branches to be combined into a single output.

General kinematic and lossless torque equations describe the operation of any type of PGS [18]:

$$\omega_3 = (1-R)\omega_2 + R\omega_1, \text{ where } R = \left(\frac{\omega_3}{\omega_1}\right)_{\omega_2=0} \tag{3}$$

$$T_{3,\,lossless} = -\left(\frac{1}{1-R}\right)T_{2,\,lossless} = -\left(\frac{1}{R}\right)T_{1,\,lossless} \tag{4}$$

For a particular PGS geometry (defined by the ratio between the number of teeth on the sun and ring gears), there are six possible values of R relating to the possible assignment of the sun, ring and carrier branches to the generic branches (1, 2 and 3) described in Equation 3. The general definition of R in Equation 3, however, means that the kinematic and torque relationships between the sun, ring and carrier branches are identical in all cases. By using the general speed and torque relationships (Equations 3 and 4) in the following analysis of flywheel systems, general algebraic expressions can be derived for system performance. Calculations can then be performed to find the R value(s) required for a particular transmission and application. This value of R allows the most appropriate PGS configuration (i.e. simple or idler), branch connections and ratio of sun-to-ring teeth to be deduced, as discussed in detail by White [18, 38]. It is therefore unnecessary to perform separate calculations for all the possible permutations of the branch connections.

A simple constant efficiency term, η_n, has been used to describe mechanical losses in a general PGS with gear ratio R_n as shown in Equation 5, where the subscripts *out* and *in* describe whether power is transferred out of or into the PGS at a particular branch. As the kinematic relationship in Equation 3 must be satisfied, this results in Equation 6 which describes the relationship between the torques at two branches where the sign of the power flow is opposite.

$$\sum(\omega T)_{out} + \eta_n \sum(\omega T)_{in} = 0 \tag{5}$$

$$\frac{T_{out}}{T_{in}} = \eta_n \left(\frac{T_{out}}{T_{in}}\right)_{lossless} \tag{6}$$

Alternatively, if two branches have the same power flow sign, the torque relationship between them is equal to the lossless case defined in Equation 4. For example, in the case where power flows into the PGS at branch 1, and out of the PGS at branches 2 and 3, the following equations apply:

$$\frac{T_2}{T_1} = \eta_n \left(\frac{1 - R_n}{R_n} \right), \quad \frac{T_3}{T_1} = -\eta_n \left(\frac{1}{R_n} \right), \quad \frac{T_3}{T_2} = -\left(\frac{1}{1 - R_n} \right) \tag{7}$$

Similar torque ratios can be derived for any combination of power flows in the three PGS branches.

4.2. Analysis of continuous-slip transmissions for flywheel systems

The simplest CST configuration is the brake-controlled PGS. The single PGS system studied by Diego-Ayala et al [32] can be extended to a multi-PGS transmission, as shown in Figure 3, and optimised. A single stage of this transmission configuration is shown schematically in Figure 5, where the PGS branches *1*, *2* and *3* are assigned to the flywheel, brake and final drive respectively. While arbitrary, this assignment of branches is convenient in the following analysis, as it allows the PGS ratio, R_n, to be directly related to the overall ratio of final drive-to-flywheel speed, r, which is an important variable. The power flow and resulting kinematic requirements for achieving charge and discharge of the flywheel are stated in Table 2.

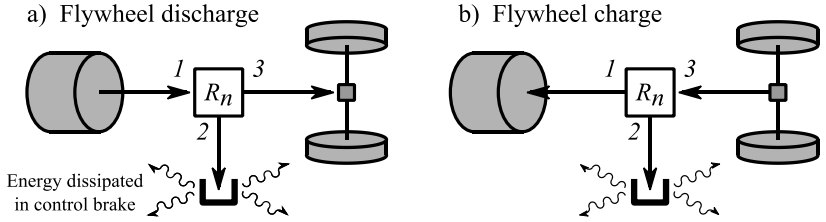

Figure 5 – Schematic illustration of brake-controlled PGS during flywheel charge and discharge

Operation:	Discharge	Charge
Power flow requirement:	$P_2/P_3 \geq 0$	$P_2/P_3 \leq 0$
Kinematic requirement:	$\frac{\omega_2}{\omega_3}(R_n - 1) \geq 0$	$\frac{\omega_2}{\omega_3}(R_n - 1) \leq 0$

Table 2 – Kinematic requirements for a phase of flywheel charge or discharge using a brake-controlled PGS (note that equality is achieved at the point when flywheel discharge or charge is no longer possible)

A 'phase' of flywheel charging or discharging is defined as the period between the start of energy dissipation in the brake (which is subject to the kinematic requirements in Table 2) and the point at which the speed of branch 2 becomes zero. It is necessary to know the amount of energy dissipated in the brake during a phase of operation in order to derive the final flywheel and vehicle speeds.

For a CST with a total number of brake-controlled PGSs equal to N, the following procedure describes how analytical expressions can be derived for the total energy transferred during operation of the n'th PGS, where subscripts i and f refer to initial and final values for the n'th phase;

i. Differentiate Equation 3 w.r.t. time, and substitute Equation 2:

$$\frac{d\omega_2}{dt} = \frac{1}{(1 - R_n)} \left(\frac{R_n T_1}{J_{fw}} - \frac{T_3}{J_{fd}} \right) \tag{8}$$

ii. Substitute torque equations into Equation 8 (shown here for the discharge case using torque relationships from Equation 7):

$$\frac{d\omega_2}{dt} = -\frac{T_2}{(1 - R_n)^2} \left(\frac{1}{J_{fd}} + \frac{R_n^{\,2}}{\eta_n J_{fw}} \right) \tag{9}$$

iii. Calculate energy dissipation in the brake by integrating power over the duration of the phase, and substitute result from step (ii):

$$\Delta E_2 = \int_{t_i}^{t_f} T_2 \omega_2 \, dt = \int_{\omega_{2,i}}^{0} T_2 \omega_2 \left(\frac{dt}{d\omega_2} \right) d\omega_2 \tag{10}$$

iv. Apply conservation of energy to the PGS:

$$\eta_{pgs,n} \Delta E_{in} + \sum \Delta E_{out} = 0 \tag{11}$$

Where: $\Delta E_1 = \frac{1}{2} J_{fw} \left({\omega_{1,f}}^2 - {\omega_{1,i}}^2 \right)$ and $\Delta E_3 = \frac{1}{2} J_{fd} \left({\omega_{3,f}}^2 - {\omega_{3,i}}^2 \right)$

v. Substitute the following equations relating the branch speeds into Equation 11 and rearrange to find expressions for ratio of final-to-initial flywheel speed for the *n*'th phase of operation:

$\omega_{3,f} = R_n \omega_{1,f}$, as $\omega_{2,f} = 0$

$\omega_{3,i} = R_{prev} \omega_{1,i}$, as $\left(\omega_{2,f} \right)_{prev} = 0$

$$\omega_{2,i} = \left(\frac{1}{1 - R_n} \right) \left(\omega_{3,i} - R_n \omega_{1,i} \right) = \left(\frac{R_{prev} - R_n}{1 - R_n} \right) \omega_{1,i}$$

For the discharge case: $R_{prev} = R_{n-1}$, where $R_0 = 0$

For the charge case: $R_{prev} = R_{n+1}$, where $R_{N+1} = \left(\omega_{fd} / \omega_{fw} \right)_{initial}$

vi. Express the flywheel speed ratio for the phase, $\left(\omega_{1,f} / \omega_{1,i} \right)_n$, in terms of a normalised PGS ratio:

$$R_n^* = R_n \sqrt{J_{fd} / J_{fw}} \tag{12}$$

The procedure described above produces the equations shown in Table 3 for a single phase of flywheel charge or discharge. The derivation of flywheel speed ratio for the discharge phase is described in detail in the Appendix.

Flywheel operation:	**Discharge**	**Charge**
Flywheel speed ratio, $\left(\omega_{1,f} / \omega_{1,i} \right)_n$:	$\frac{R_n^* R_{n-1}^* + \eta_n}{\left(R_n^* \right)^2 + \eta_n}$	$\frac{\eta_n R_n^* R_{n+1}^* + 1}{\eta_n \left(R_n^* \right)^2 + 1}$
Transmission torque ratio, $\left(T_{fd} / T_{fw} \right)_n$:	$-\frac{\eta_n}{R_n}$	$-\frac{1}{\eta_n R_n}$

Table 3 – Equations for the *n*'th operating phase of a CST consisting of multiple brake-controlled PGSs

For either charge or discharge cases, the final flywheel and vehicle speed from one phase are the initial speeds for the following phase. The 'flywheel speed ratio' equations shown in Table 3 can therefore be applied sequentially in order to calculate the overall change in kinetic energy of both the flywheel and vehicle for a system with *N* planetary gear sets once all values of R_n^* (for *n* = 1 to *N*) have been specified.

In order to characterise the overall performance of a multi-phase transmission, full charge and full discharge events can be defined as follows;

- A full discharge event is defined as the use of a fully charged flywheel to accelerate the vehicle from stationary until the transmission reaches its maximum possible ratio and the flywheel speed reaches its minimum value.

- A full charge event is defined as the deceleration of the vehicle to a standstill from an initial speed, $\omega_{fd,\,0}$, that achieves full recharge of the flywheel from its minimum to its maximum speed. Note that this initial condition defines $R_{N+1}=\omega_{fd,\,0}/\omega_{fw,\,\min}$. No further charging is possible if $\omega_{fd} \le R_1\omega_{fw}$, and conventional braking must then be used to bring the vehicle to a stop.

The variation in flywheel and vehicle speed with time for full charge and discharge events is illustrated in Figure 6 for a general case with constant torque at the final drive.

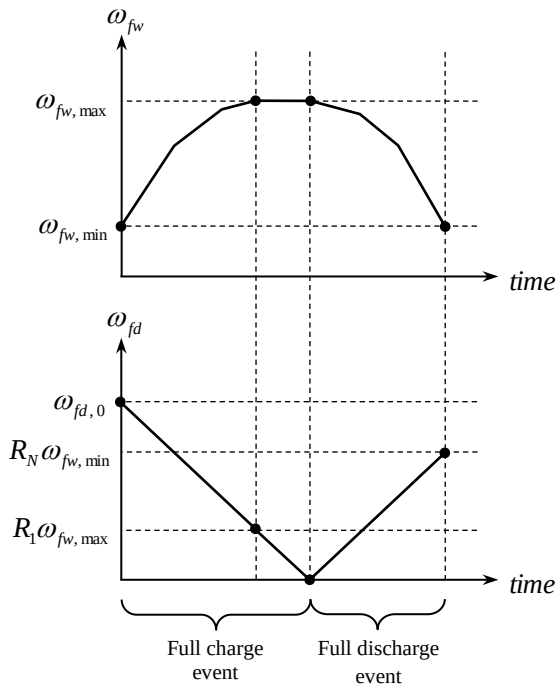

Figure 6 – Illustration of the variation in speed of the flywheel and final drive for full charge and full discharge events

The instantaneous transmission efficiency during a phase of operation can be defined in relation to the overall speed ratio, *r*, as follows;

$$\eta_{trans,\,dis} = -r\left(\frac{T_{fd}}{T_{fw}}\right)_{dis} \text{ and } \eta_{trans,\,ch} = -\frac{1}{r}\left(\frac{T_{fw}}{T_{fd}}\right)_{ch}, \text{ where } r = \frac{\omega_{fd}}{\omega_{fw}} \tag{13}$$

It is also possible to define a mean energy efficiency for full charge and full discharge events. This is simply the overall energy transfer efficiency, which for a discharge event equals the kinetic energy delivered to the vehicle divided by the kinetic energy removed from the flywheel. It therefore only depends on the initial and final speeds of the vehicle and flywheel and their inertias, and can be expressed in terms of the overall depth-of-discharge and the R_N^* and R_{N+1}^* values as shown in equations 14 and 15. The efficiency of the PGS will affect the depth-of-discharge that is achieved using particular R^* values (as can be seen from the 'flywheel speed ratio' equations in Table 3), thereby influencing the average transmission efficiency.

$$\overline{\eta}_{dis} = \left(\frac{\Delta E_{fd}}{\Delta E_{fw}}\right)_{dis} = \frac{J_{fd}\left(R_N\omega_{fw,\,\min}\right)^2}{J_{fw}\left(\omega_{fw,\,\max}{}^2 - \omega_{fw,\,\min}{}^2\right)} = \left(\frac{1-\lambda}{\lambda}\right)\left(R_N^*\right)^2 \tag{14}$$

$$\overline{\eta}_{ch} = \left(\frac{\Delta E_{fw}}{\Delta E_{fd}}\right)_{ch} = \frac{J_{fw}\left(\omega_{fw,\,\max}{}^2 - \omega_{fw,\,\min}{}^2\right)}{J_{fd}\left(\omega_{fd,\,0}\right)^2} = \left(\frac{\lambda}{1-\lambda}\right)\left(\frac{1}{R_{N+1}^*}\right)^2, \text{ where } R_{N+1}=\frac{\omega_{fd,\,0}}{\omega_{fw,\,\min}} \tag{15}$$

The mean charge-discharge cycle efficiency, $\overline{\eta}_{cyc}$, refers to the ratio of the vehicle braking energy required for full charge to the traction energy delivered to the vehicle during full discharge;

$$\overline{\eta}_{cyc} = \frac{\left(\Delta E_{fd}\right)_{dis}}{\left(\Delta E_{fd}\right)_{ch}} = \overline{\eta}_{ch}\overline{\eta}_{dis} \tag{16}$$

For a full discharge event using a brake-controlled CST consisting of N PGSs, the transmission efficiency and overall flywheel depth-of-discharge can be found once the N values of R^* have been specified. Multi-variable optimization has been performed to identify the R^* values that result in maximum mean discharge efficiency as a function of λ for a range of systems. These optimum R^* values are shown in Figure 7 for the case of a 4-PGS brake-controlled CST, and Figure 8 shows the instantaneous charge and discharge efficiency for this transmission when $\lambda = 0.8$. Figure 9 shows the variation of discharge efficiency and charge-discharge cycle efficiency with λ for a range of brake-controlled CSTs with 1-8 PGSs.

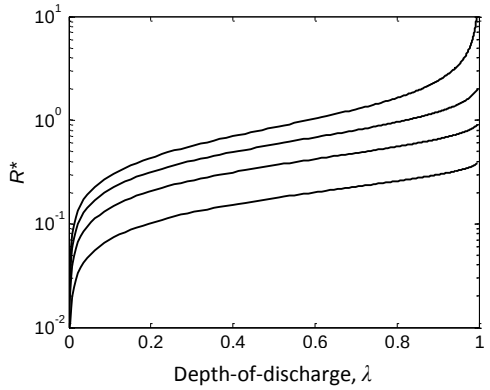

Figure 7 – Values of R^* that maximise mean discharge efficiency for a 4 PGS brake-controlled CST

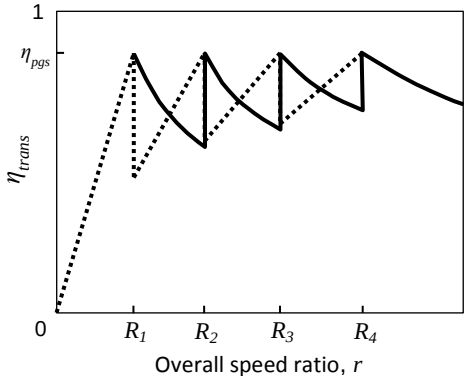

Figure 8 – Instantaneous transmission efficiency during charge (solid line) and discharge (dotted line) as a function of overall speed ratio, r, for a 4 PGS brake-controlled CST with $\lambda = 0.8$

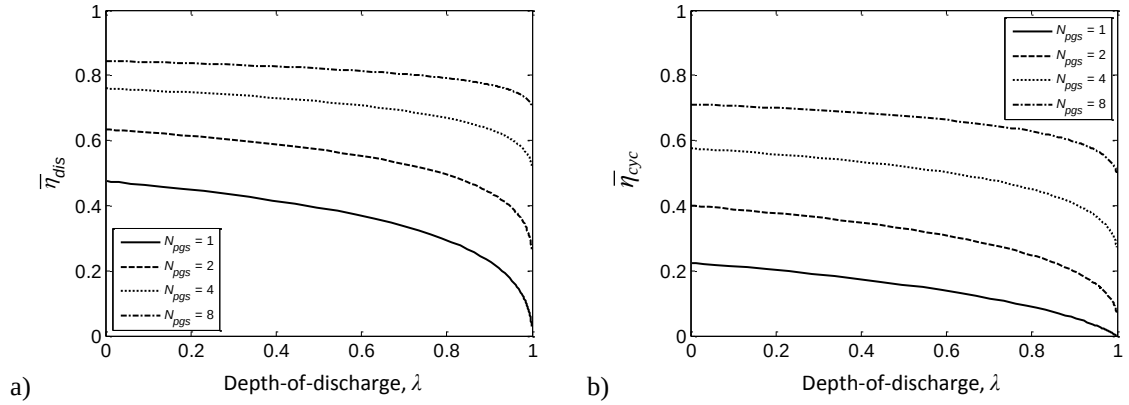

a) b)

Figure 9 – a) Maximum mean discharge and b) charge-discharge cycle efficiency as a function of λ for flywheel systems with various brake-controlled CSTs

Figure 9 shows that increasing the number of PGSs in the brake-controlled CSTs, and therefore the number of phases of operation during charge and discharge, increases the transmission efficiency for a given λ. There are however practical constraints on the cost, mass and complexity of the transmission, which will limit the number of PSGs that can be used in a practical system. An alternative is to implement a power-split configuration to increase the number of phases of operation that can be achieved in the transmission. This is discussed in the following Section.

4.3. Continuous-slip transmissions with power-split

The concept of continuous-slip transmissions can be extended by considered power-split configurations. These can be implemented by connecting a counter-shaft gearbox to one or more PGSs; this is achieved without power recirculation to ensure that the power flow in the counter-shaft gearbox is less than the transmission input power. This arrangement results in a compact transmission with a large number of discrete ratios, making it suitable as a continuous-slip flywheel transmission.

Two basic modes of power-split are implemented in this type of transmission; final drive coupled (FDC) and dual differential coupled (DDC). These are illustrated in Figures 10 and 11 respectively, with the power flow direction shown for the case of flywheel discharge. In the case of charging, the power flow direction in all shafts is reversed. This reversal of power flow between flywheel charge and discharge is the reason that the more conventional 'input coupled' and 'output coupled' descriptions of power-split configuration have been avoided.

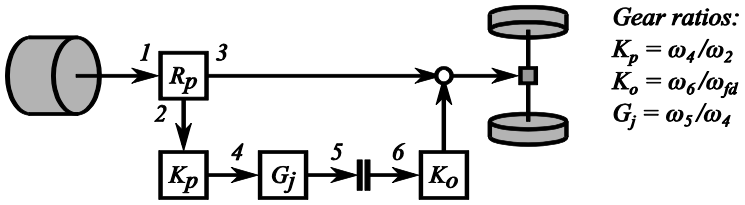

Figure 10 – Schematic diagram of FDC power-split configuration, with power flow shown for flywheel charging

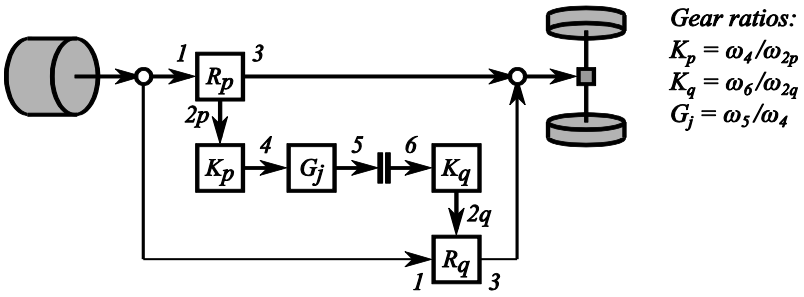

Figure 11 – Schematic diagram of DDC power-split configuration, with power flow shown for flywheel discharge when $R_p/R_q > 1$ (note that if $R_q/R_p > 1$ the direction of power flow in shaft *2p*, *4*, *5*, *6* and *2q* is reversed)

In both the FDC and DDC cases illustrated in Figures 10 and 11, for a particular CGB gear ratio, G_j, discharge of the flywheel can be achieved by applying a torque via sliding contact in the clutch as long as $(\omega_5/\omega_6) > 1$. Likewise, flywheel charging can only be achieved while $(\omega_6/\omega_5) > 1$. In both cases, power flow stops once the slip speed in the clutch reaches zero ($\omega_5 = \omega_6$), at which point the overall transmission ratio becomes fixed.

For both FDC and DDC power-split modes the operation is essentially the same as for the brake-controlled PGS illustrated in Figure 5, as;

i. A proportion of the energy entering the transmission during a phase of operation is dissipated in the control element (either the PGS brake or the CGB clutch).

ii. Power transfer continues with a constant torque ratio between the flywheel and final drive until the slip speed in the control element reaches zero. At this point, the transmission has a fixed speed ratio between the flywheel and final drive.

The difference is that with the FDC and DDC power-split modes;

i. The gearing losses depend on the efficiency of the CGB as well as the efficiency of the PGS(s).

ii. The final transmission ratio achieved in each phase depends on the fixed gear ratio of the CGB and associated gearing as well as the characteristic ratio of the PGS(s)

The equations described in Table 3 can therefore be applied to transmissions with FDC and DDC power-split modes using an equivalent characteristic ratio and efficiency during charge and discharge, defined as shown in Figure 12.

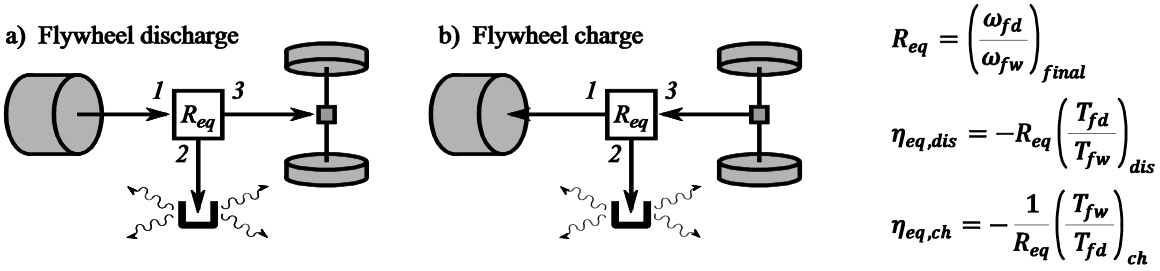

Figure 12 – Schematic illustration of equivalent brake-controlled PGS and the definition of equivalent values that can be used to characterise a phase of operation of FDC and DDC power split modes

The derivation of these equivalent expressions is illustrated below for the FDC case by considering the speed and torque relationships in the transmission.

The overall transmission speed ratio for the FDC configuration when slip speed in the clutch equals zero can be found by combining Equation 3 with gear ratio equations in Figure 10:

$$R_{eq} = R_{FDC} = \left(\frac{\omega_{fd}}{\omega_{fw}}\right)_{\omega_5=\omega_6} = R_p\left(1-\left(1-R_p\right)\frac{K_{fd}}{G_j K_p}\right)^{-1} \tag{17}$$

Note that in order to achieve the required power flow during flywheel charge or discharge for the FDC transmission configuration shown in Figure 10, $(P_3/P_2) > 0$ and $(\omega_5/\omega_6) > 0$. Therefore;

$$\left(1-R_p\right)\frac{K_{fd}}{G_j K_p} < 0, \text{ and from Equation 17, } 0 < \frac{R_{FDC}}{R_p} < 1 \tag{18}$$

From Equation 18 it is apparent that a phase of FDC operation using a particular CGB gear ratio is equivalent to a brake-controlled PGS with an R value between zero and R_p.

The overall transmission torque ratio for the FDC transmission during flywheel charge and discharge can be found by combining the PGS torque equations with gear ratio equations in Figure 10, using a constant efficiency, η_{cgb}, for the control gear, G_j:

$$\left(\frac{T_{fd}}{T_{fw}}\right)_{FDC,\,dis} = \frac{\eta_p}{R_p}\left(\eta_{cgb}\left(1-R_p\right)\frac{K_{fd}}{G_j K_p}-1\right) = \frac{\eta_p}{R_p}\left(\eta_{cgb}\left(1-\frac{R_p}{R_{FDC}}\right)-1\right) \tag{19}$$

$$\left(\frac{T_{fd}}{T_{fw}}\right)_{FDC,\,ch} = \frac{1}{\eta_p R_p}\left(\frac{1}{\eta_{cgb}}\left(1-\frac{R_p}{R_{FDC}}\right)-1\right) \tag{20}$$

Using the definitions in Figure 12, the equivalent charge and discharge efficiencies for the FDC power split mode are as follows:

$$\eta_{eq,\,dis} = \eta_{FDC,\,dis} = -R_{FDC}\left(\frac{T_{fd}}{T_{fw}}\right)_{FDC,\,dis} = \eta_p\left(\eta_{cgb} + \left(\frac{R_{FDC}}{R_p}\right)\left(1-\eta_{cgb}\right)\right) \tag{21}$$

$$\eta_{eq,\,ch} = \eta_{FDC,\,ch} = -\frac{1}{R_{FDC}}\left(\frac{T_{fw}}{T_{fd}}\right)_{FDC,\,ch} = \eta_p\eta_{cgb}\left(1-\left(\frac{R_{FDC}}{R_p}\right)\left(1-\eta_{cgb}\right)\right)^{-1} \tag{22}$$

This is a particularly useful result as it allows the performance of the FDC transmission to be calculated using the equations previously derived for the brake-controlled PGS transmission. Similar expressions can be derived for the DDC power split mode described in Figure 11:

$$R_{DDC} = \left(\frac{\omega_{fd}}{\omega_{fw}}\right)_{\omega_5=\omega_6} = \left(R_p - R_q\frac{\left(1-R_p\right)}{\left(1-R_q\right)}\frac{K_q}{G_j K_p}\right)\left(1-\frac{\left(1-R_p\right)}{\left(1-R_q\right)}\frac{K_q}{G_j K_p}\right)^{-1} \tag{23}$$

$$\eta_{DDC,\,dis} = \eta_p\left(1+\eta_q\eta_{cgb}\left(\frac{R_p - R_{DDC}}{R_{DDC} - R_q}\right)\right)\left(\left(\frac{R_p}{R_{DDC}}\right)+\eta_p\eta_{cgb}\left(\frac{R_q}{R_{DDC}}\right)\left(\frac{R_p - R_{DDC}}{R_{DDC} - R_q}\right)\right)^{-1} \tag{24}$$

$$\eta_{DDC,\,ch} = \eta_q\left(\eta_p\eta_{cgb}\left(\frac{R_p}{R_{DDC}}\right)+\left(\frac{R_q}{R_{DDC}}\right)\left(\frac{R_p - R_{DDC}}{R_{DDC} - R_q}\right)\right)\left(\eta_q\eta_{cgb}+\left(\frac{R_p - R_{DDC}}{R_{DDC} - R_q}\right)\right)^{-1} \tag{25}$$

Note that in order to achieve the required power flow during flywheel charge or discharge for the DDC transmission configuration shown in Figure 11, $(P_{2p}/P_{2q}) < 0$ and $(\omega_5/\omega_6) > 0$. Therefore,

$$\frac{\left(1-R_p\right)}{\left(1-R_q\right)}\frac{K_q}{G_j K_p} < 0 \tag{26}$$

Substituting Equation 26 into Equation 23 results in the following relationships:

$$\text{If } \frac{R_p}{R_q} > 1 \text{ then } \frac{R_q}{R_p} < \frac{R_{DDC}}{R_p} < 1, \text{ and if } \frac{R_q}{R_p} > 1 \text{ then } \frac{R_q}{R_p} > \frac{R_{DDC}}{R_p} > 1 \tag{27}$$

From Equation 27 it is apparent that a phase of DDC operation using a particular CGB gear ratio is equivalent to a brake-controlled PGS with an R value between R_q and R_p.

Equations 24 and 25 only apply to the case when $R_p/R_q > 1$, as shown in Figure 11. In cases where $R_q/R_p > 1$, the expression for R_{DDC} (Equation 23) remains the same, while the correct equivalent PGS efficiencies for charge and discharge can be found by swapping the p and q subscripts in Equations 24 and 25.

For the flywheel transmission application considered here, the results in Table 3 and Equations 17, 21-25 show that (like the brake controlled transmissions) the operation of a CGB controlled transmission consisting of FDC and DDC power split modes is characterised only by the actual and equivalent R^* values and the gearing efficiencies. However, unlike the brake controlled transmissions, CGB controlled PSTs have an additional kinematic constraint as the values of R_{eq}^* in each of the power-split modes must be consistent with the fixed discrete CGB gear ratios, G_j, (where j = 1 to N_{cgb}). This means that the values of R_{eq}^* in different power-split modes are not independent. The performance of a given CGB controlled PST configuration can be analysed by specifying the actual R^* values for the PGS(s), a single R_{eq}^* value for each of the power-split modes, and all values of G_j/G_1 for the CGB. The unspecified values of R_{eq}^* can then be calculated using equations 17 and 23 (for FDC and DDC power split modes respectively), and optimisation of the transmission gearing ratios can be performed to identify the maximum possible mean discharge efficiency as a function of λ.

Figure 13 shows the R^* values (both actual and equivalent) required to achieve maximum mean discharge efficiency, and the associated CGB gear ratios, for a particular transmission consisting of 2 PGSs and a 4-speed CGB. The relationship between the CGB gear ratios illustrates a general result that the ratio of maximum to minimum G values (G_4/G_1 in this example) is approximately equal to the square of the total number of gear ratios in the CGB. A sensible upper limit for the gear ratio that can be achieved in a single gear pair is around 4:1, and to ensure that a simple counter-shaft design can be used for the CGB the maximum number of gears has therefore been limited to 4. The maximum mean discharge and charge-discharge cycle efficiencies are shown in Figure 14 for a range of flywheel systems with 4-speed CGB controlled transmissions.

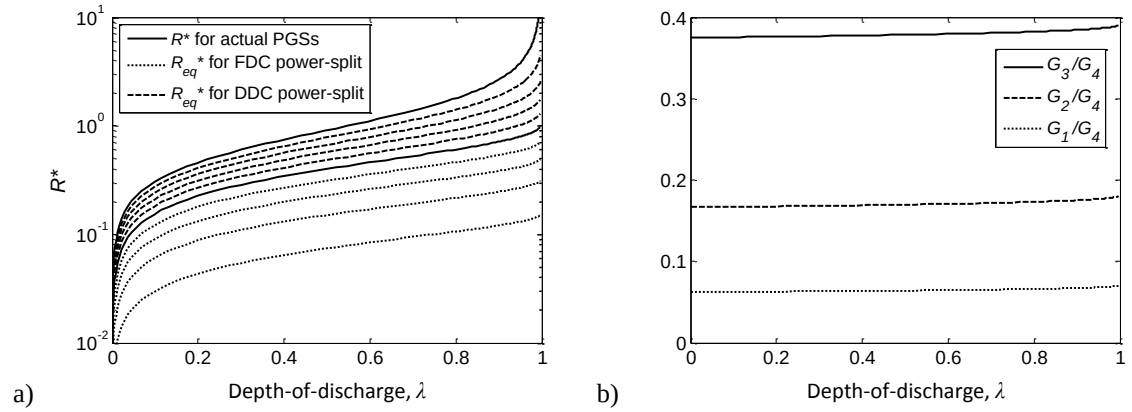

a) b)

Figure 13 – a) Actual and equivalent R^* values and b) the associated G_j/G_4 values required to achieve maximum discharge efficiency using a 2 PGS, 4-speed CGB controlled transmission (η_{pgs} = 95%, η_{cgb} = 95%)

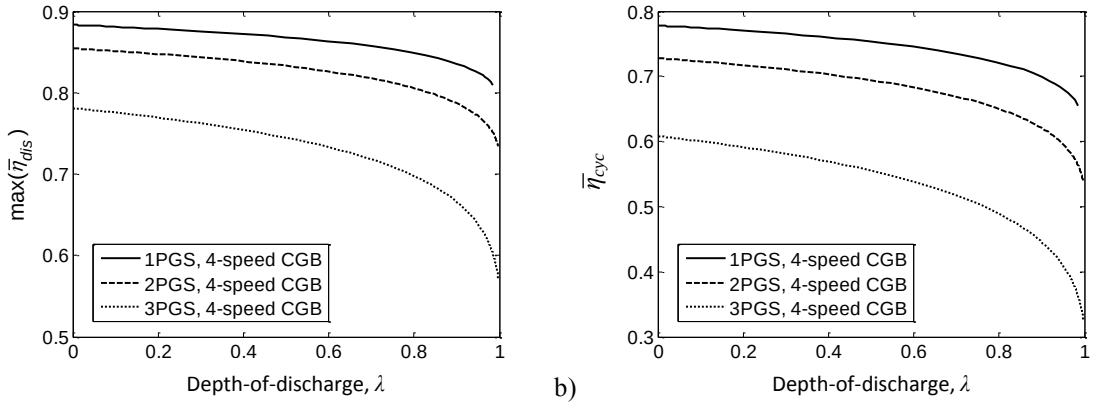

a) b)

Figure 14 – a) Maximum discharge efficiency and b) associated charge-discharge cycle efficiency for a flywheel system with various CGB controlled transmissions (η_{pgs} = 95%, η_{cgb} = 95%)

5. Selection of suitable flywheel system parameters for practical applications

It has been shown that maximum discharge efficiency and the required gear ratios for a particular application can be identified as a function of λ. There is, however, an inherent compromise between high mean transmission efficiency (which occurs at low λ) and a compact flywheel (which requires high λ). It is therefore necessary to identify a sensible λ for the flywheel system that achieves a good balance between high efficiency and low system mass; all system components must be considered, as the transmission can account for a significant proportion of the overall system mass. Therefore, the total system mass is essential to identifying appropriate parameters for a particular system configuration and application.

It is possible to estimate the total mass of the flywheel system as a function of λ for a particular application; this system mass is the sum of the mass of the flywheel, PGS(s) and CGB components. For the flywheel and PGS(s) the mass can be estimated by using representative values of specific energy capacity ($\overline{E}_{fw}$) and specific torque capacity ($\overline{T}_{pgs}$) respectively, as shown in Equation 28. Identifying the total system mass allows the system parameters to be selected that achieve the lowest system mass per unit of energy transferred to the vehicle during flywheel discharge, defined as the system specific energy capacity, $\overline{E}_{sys}$, in Equation 29.

$$m_{sys} = m_{fw} + m_{pgs} + m_{cgb} = \frac{E_{fw,\max}}{\overline{E}_{fw}} + \sum_{1}^{N_{pgs}} \frac{T_{pgs,\max}}{\overline{T}_{pgs}} + m_{cgb} \tag{28}$$

$$\overline{E}_{sys} = \frac{\left(\Delta E_{fd}\right)_{dis}}{m_{sys}} = \frac{\frac{1}{2} J_{fd} \omega_{fd,0}{}^2 \overline{\eta}_{rt}}{m_{sys}} \tag{29}$$

In order to calculate the mass of the CGB component for power-split transmissions, it is necessary to assess the torque and speed that occur at the input and output of the CGB during full charge and full discharge events.

The instantaneous torque and speed that occur at shaft 5 (as defined in Figures 10 and 11) can be normalised by the torque and speed at the final drive, and the gear ratio, K_o, that connects the CGB to the final drive in the FDC mode of operation. Expressions for the normalised torque and speed are shown in Equations 30 and 31 respectively. These normalised variables are purely functions of the actual and equivalent R^* values, and can be calculated as a function of the overall speed ratio of the transmission during operation for a given λ, as illustrated in Figure 15.

$$T_5^* = \left| K_o \frac{T_5}{T_{fd}} \right| \tag{30}$$

$$\omega_5^* = \left| \frac{1}{K_o} \frac{\omega_5}{\omega_{fd,\max}} \right|, \text{ where } \omega_{fd,\max} = \omega_{fd,0} \text{ (i.e. the initial speed for a full recharge event)} \tag{31}$$

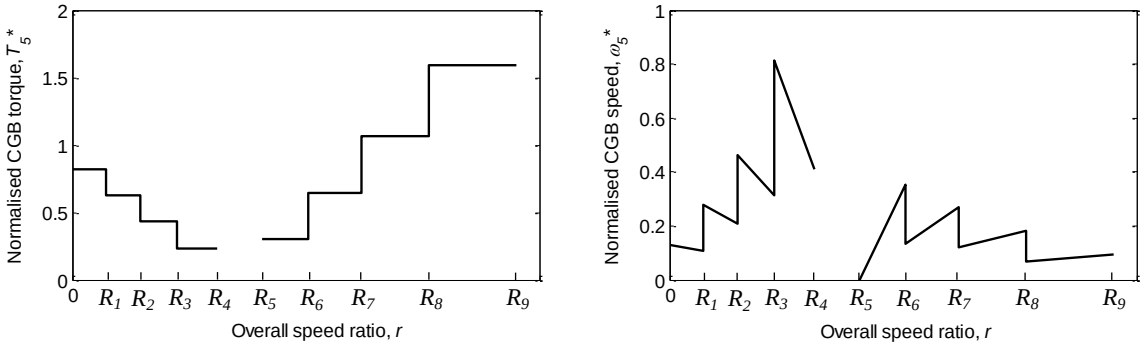

Figure 15 – Variation of T_5^* and ω_5^* with r for the particular case of flywheel discharge using 2-PGS, 4-CGB transmission sized for $\lambda = 0.8$ (where R_1-R_4 and R_6-R_9 are the equivalent ratios for phases of FDC and DDC operation respectively)

The instantaneous torque and speed that occur at shaft 4 (as defined in Figures 10 and 11) depend on the CGB gear ratios, as shown below:

$$T_4^* = \left| \eta_{cgb} G_j T_5^* \right| \text{ or } \left| \left(G_j T_5^* \right) / \eta_{cgb} \right| \text{ depending on the direction of power flow} \tag{32}$$

$$\omega_4^* = \left| \omega_5^* / G_j \right| \tag{33}$$

For specified values of G, the maximum normalised speed, ω_{cgb}^*, and torque, T_{cgb}^*, that occur at either the input or output of the CGB during either a full discharge or full recharge event can be identified as functions of λ. If it is assumed that the maximum required torque at the final drive, $T_{fd,\max}$, can be achieved at any point during flywheel charge or discharge, then a normalised power rating for the CGB, P_{cgb}^*, can be defined as shown in Equation 34. The maximum normalised CGB speed and the normalised rated power as functions of λ are illustrated in Figure 16 for a flywheel system using a 2-PGS, 4-CGB transmission.

$$P_{cgb}^* = \left| \frac{T_{cgb,\max} \omega_{cgb,\max}}{T_{fd,\max} \omega_{fd,\max}} \right| = \max\left(T_{cgb}^* \right) \max\left(\omega_{cgb}^* \right) \tag{34}$$

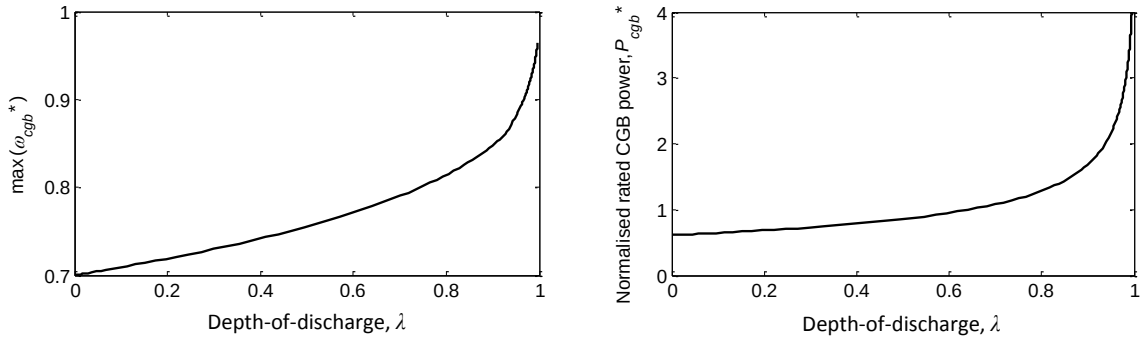

Figure 16 – Variation of $\max\left(\omega_{cgb}^{*}\right)$ and P_{cgb}^{*} as functions of λ for 2-PGS, 4-CGB transmission with $G_1 = 0.25$

The maximum rotational speed that is allowed at the CGB, $\omega_{cgb,\max}$, can be specified according to the gearbox design. The flywheel system can be sized for a particular application such that a typical braking event is sufficient to fully recharge the flywheel, thereby defining the required value of $\omega_{fd,\max}$. Rearranging Equation 34 therefore enables the maximum CGB torque, $T_{cgb,\max}$, to be assessed as a function of λ for a given application.

$$T_{cgb,\max} = P_{cgb}^{*}\left(\frac{T_{fd,\max}\omega_{fd,\max}}{\omega_{cgb,\max}}\right) \tag{35}$$

The mass of the CGB can be calculated using an empirical relationship derived for passenger car gearboxes by Naunheimer et al [39], where the gearbox mass, m_{gb}, is characterised as a function of the maximum torque and the number of gear ratios as shown in Equation 36.

$$m_{gb} = 0.199\left(T_{gb,\max}{}^{0.669} N_{gb}{}^{0.334}\right) \tag{36}$$

This empirical relationship has been derived for passenger car transmissions, where the maximum speed is similar to the maximum engine speed. The maximum allowable speed for the CGB has therefore been specified as 5000 rpm. When used to calculate the mass of a CGB, the total number of speeds has been specified so as to include the fixed gear ratios that connect the CGB to the PGS(s) and the final drive, resulting in Equation 37.

$$m_{cgb} = 0.199\left(T_{cgb,\max}{}^{0.669}\left(N_{cgb} + N_{pgs} + 1\right)^{0.334}\right) \tag{37}$$

A particular flywheel application is defined by the maximum torque and speed required at the final drive and the vehicle inertia. Specified values of $\omega_{cgb,\max}$ and λ are used to find the required values of K_o and $T_{cgb,\max}$ from Figure 16. This allows transmission gear ratios to be specified and the CGB mass to be calculated using Equation 37. The required flywheel capacity, gearing ratios, total system mass (Equation 28) and the specific energy capacity of the system (Equation 29) can therefore be calculated for a particular application. This is described for the example of a passenger car in the following Section.

5.1. Example of flywheel system sizing for a passenger car application

The following analysis of flywheel systems has been performed using characteristic data for a medium sized passenger car. A typical braking event for this application has been defined as a deceleration from 48 km/h to stationary, as found in the ECE 15 urban drive cycle, and the maximum acceleration has been specified as $\pm 1 \text{m/s}^2$. The vehicle can be characterised using the expressions in Equation 37, and the data required for this application is presented in Table 4.

$$\omega_{fd} = \left(\frac{K_{fd} v_{veh}}{r_w}\right),\ J_{fd} = m_{veh}\left(\frac{r_w}{K_{fd}}\right)^2 \text{ and } T_{fd,\max} = m_{veh} a_{\max}\left(\frac{r_w}{K_{fd}}\right) \tag{38}$$

Vehicle mass (kg)	m_{veh}	1500
Radius of wheels (m)	r_w	0.282
Final drive ratio	K_{fd}	3.84
Maximum torque required at final drive (Nm)	$T_{fd,\max}$	100

Maximum allowable CGB speed (rpm)	$\omega_{cgb,\,\max}$	5000
Typical initial vehicle braking speed (km/h)	$v_{veh,\,\max}$	48
CGB efficiency	η_{cgb}	0.95
PGS efficiency	η_{pgs}	0.95
Flywheel specific energy capacity (kJ/kg)	$\overline{E}_{fw}$	50
PGS specific torque (Nm/kg)	$\overline{T}_{pgs}$	50

Table 4 – Data used in analysis of flywheel system performance for a passenger car application

The mass of individual components and the specific energy of the flywheel system can be calculated for the particular application, and an example is shown in Figure 17 for a system using a 2-PGS, 4-CGB transmission. With reference to Equation 29, maximum specific energy represents a good compromise between high efficiency and low system mass. This is seen to occur at $\lambda = 0.66$ for the system in Figure 17, and the system parameters required to achieve this are shown in Table 5.

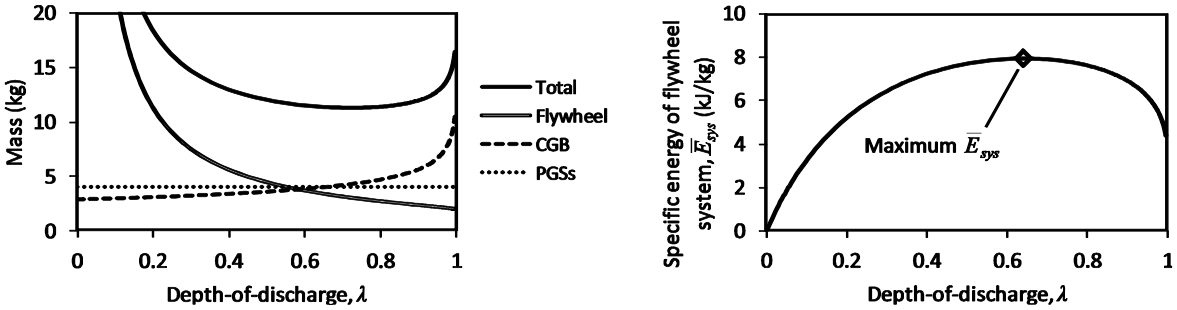

Figure 17 – Mass of components and specific energy of flywheel system as functions of λ using a 2-PGS, 4-CGB transmission for the passenger car application defined in Table 1

Depth-of-discharge	λ	0.640
Specific energy of flywheel system (kJ/kg)	$\overline{E}_{sys}$	7.85
Mean discharge efficiency	η_{dis}	0.823
Mean charge-discharge cycle efficiency	η_{cyc}	0.678
Flywheel capacity (kJ)	$E_{fw,\,\max}$	171
CGB gear ratios	G_1	-0.25
	G_2	-0.66
	G_3	-1.46
	G_4	-3.84
CGB-to-final drive gear ratio	K_o	-3.70
General requirements for PGS ratios	R_A^*	±0.486
	R_B/R_A	2.49

Table 5 – Specification for flywheel system (using a 2-PGS, 4-CGB transmission) sized to achieve maximum specific energy for the passenger car application defined in Table 1

The general PGS ratio requirements shown in Table 5 must be satisfied. This requires a value of R_A to be chosen that will determine R_B and the required flywheel inertia, hence the maximum flywheel speed. Table 6 shows one possible specification for the PGSs. This configuration achieves the lowest absolute value of R_A (hence the highest maximum flywheel speed) that is possible for a practical coaxial arrangement of PGSs using the practical limitations for single stage simple and idler gearing types identified by White [38], where the ring-to-sun teeth ratio should be within the range of 2-3.5. The chosen PGS ratios result in a maximum flywheel speed of 360 rad/s, and the use of a higher speed flywheel will require additional gearing to match the transmission speed requirement (e.g. a 1000 rad/s flywheel needs a 3.8:1 gear ratio). This could be avoided if a

two-stage compound PGS is used to achieve a lower absolute value of R_A, although this will affect the efficiency and complexity of the transmission.

PGS:	**A**	**B**
R	-0.286	-0.712
Type (see Figure 4)	Simple	Idler
Ring-to-sun teeth ratio, n_r/n_s	3.50	2.41
Flywheel branch connection	Sun	Sun
Vehicle branch connection	Ring	Carrier
PGS-to-CGB gear ratio, K	-4.24	-4.88
Inertia ratio, J_{fd}/J_{fw}	2.89	
$\omega_{fw,\,max}$ (rad/s)	429	

Table 6 – Ratio and configuration of PGSs for flywheel system using 2-PGS, 4-CGB transmission, when chosen to achieve the highest possible $\omega_{fw,\,max}$ with single stage, coaxial PGSs

The maximum achievable specific energy capacity shown in Figure 17 for the system with a 2-PGS, 4-CGB transmission can also be found for flywheel systems using different transmission configurations. Figure 18 shows a comparison of different systems by plotting maximum specific energy capacity against the associated charge-discharge cycle efficiency. Improvements in efficiency can be achieved through increased mechanical complexity of transmissions, while the CGB controlled transmissions are seen to achieve a significantly higher specific energy capacity.

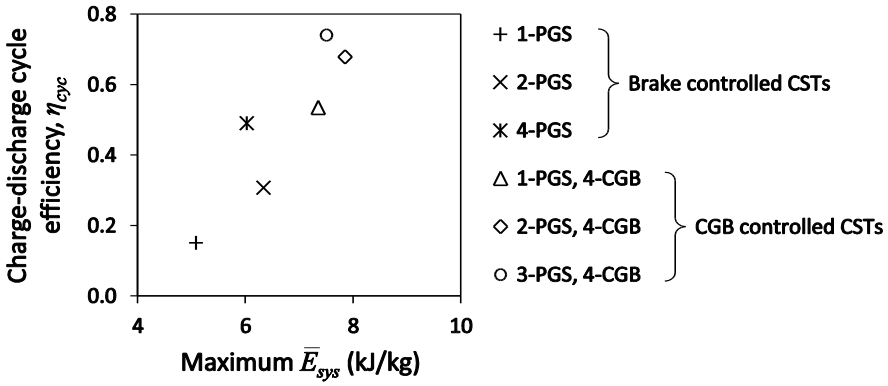

Figure 18 – Comparison of maximum specific energy capacity and associated charge-discharge cycle efficiency for optimised flywheel systems using a range of brake and CGB controlled transmissions

The importance of this analysis is that it allows a flywheel system to be appropriately sized for a particular application. The system parameters identified here should be used in more detailed analysis of the vehicle performance to quantify and compare the benefits of a range of systems in terms of emissions and fuel savings. While the results in Figure 18 provide a simple means of comparing the performance of different systems, detailed design of the flywheel and transmission also needs to be considered in order to identify an appropriate solution. This can potentially feed back into the optimisation through improved estimates of specific flywheel energy capacity and transmission mass. While specific energy capacity has been used as the optimisation target function, the same analysis method could potentially be used to optimise flywheel systems based on cost or size.

It is interesting to compare the results obtained for the brake and CGB controlled systems shown in Figure 18 with published data for the commercialised 'Flybrid' flywheel energy storage system described by Brockbank and Cross [10, 14, 15], which uses a direct toroidal CVT transmission. The Flybrid system has a significantly larger flywheel maximum kinetic energy (590kJ) than the systems shown in Figure 18. The stated system mass and round-trip efficiency of the Flybrid system are shown in Table 7. This is compared with the 2-PGS, 4-speed CGB controlled transmission, where the analysis has been performed using the data in Table 4 except with a

higher initial vehicle braking speed in order to match this higher flywheel energy capacity. As it is not stated, the depth of discharge for the flywheel in the Flybrid system has been estimated at 75%.

Flywheel system	η_{dis}	η_{cyc}	λ	m_{sys}	$\bar{E}_{sys}$
	-	-	-	Kg	kJ/kg
Flybrid direct CVT [10]	86%	74%	75% (estimate)	25	15.3
2-PGS, 4-CGB	81%	66%	78%	23.4	15.9

Table 7 – Comparison of commercialised Flybrid system and proposed 2-PGS, 4-speed CGB controlled system (sized for maximum $\bar{E}_{sys}$) using a 590 kJ flywheel

The efficiency of the CGB controlled system is shown in Table 7 to be significantly lower than the Flybrid system. It is however worth noting that the stated efficiency of the Flybrid system is essentially an upper limit as it only applies to energy transfer within the CVTs range of gear ratios, and does not include the losses that occur if the clutch is allowed to slip in order to deliver power to the vehicle at low speeds. While a more detailed analysis of both systems is necessary for a rigorous comparison, the results suggest that the efficiency, mass and specific energy of the two systems are broadly similar. The performance of flywheel systems using a range of flywheel transmissions with CVTs in both direct and power-split configurations is currently being studied using the method described in this paper, and will be presented in a future publication.

6. Conclusions

The new method described here for the analysis of mechanical flywheel hybrid vehicles has been shown to provide fundamental insight into the effect of gearing ratios on transmission efficiency, achievable overall depth-of-discharge and the mass of transmission components. The non-dimensional results of this analysis provide a design tool which can be used to characterise flywheel systems for appropriate regenerative braking applications. For a passenger car and urban drive cycle application, round-trip efficiencies of up to 75% have been predicted for flywheel systems using practical power-split transmissions controlled by a fixed ratio gearbox. This is combined with low predicted system mass of around 11kg when sized to receive around 130kJ of vehicle braking energy. These results allow an initial assessment of system performance and the specification of suitable design parameters, providing a rigorous basis for more detailed analysis of appropriate flywheel systems. This could include time-step based vehicle modelling to understand the effect of vehicle resistance, flywheel self-discharge losses and system control strategy on vehicle fuel consumption for realistic drive cycles. Future research can also focus on an accurate analysis of component mass and cost based on comprehensive design work, while consideration must also be given to the control requirements of the continuous slip transmissions described, in order to determine whether they are a practical option for flywheel energy storage systems.

Appendix

Derivation of equations for brake-controlled PGS during a phase of discharge (numerals correspond to description of procedure in Section 4.2):

ii) $$\frac{d\omega_2}{dt} = -\frac{T_2}{(1-R)^2}\left(\frac{1}{J_{fd}} + \frac{R^2}{\eta_{pgs,n} J_{fw}}\right)$$

iii) $$\Delta E_2 = (1-R)^2\left(\frac{1}{J_{fd}} + \frac{R^2}{\eta_{pgs,n} J_{fw}}\right)^{-1} \int_{\omega_{2,i}}^{0} -\omega_2 \; d\omega_2 = \frac{{\omega_{2,i}}^2}{2}\left(\frac{\eta_{pgs,n} J_{fw} J_{fd} (1-R)^2}{\eta_{pgs,n} J_{fw} + J_{fd} R^2}\right)$$

iv) $\eta_{pgs,n}\Delta E_1 + \Delta E_2 + \Delta E_3 = 0$ for flywheel discharge

$$\eta_{pgs,n} J_{fw} \left({\omega_{1,f}}^2 - {\omega_{1,i}}^2 \right) + {\omega_{2,i}}^2 \left(\frac{\eta_{pgs,n} J_{fw} J_{fd} (1-R)^2}{\eta_{pgs,n} J_{fw} + J_{fd} R^2} \right) + J_{fd} \left({\omega_{3,f}}^2 - {\omega_{3,i}}^2 \right) = 0$$

v) $$\eta_{pgs,n} J_{fw} \left({\omega_{1,f}}^2 - {\omega_{1,i}}^2 \right) + {\omega_{1,i}}^2 \left(\frac{R_{prev} - R_n}{1 - R_n} \right)^2 \left(\frac{\eta_{pgs,n} J_{fw} J_{fd} (1-R_n)^2}{\eta_{pgs,n} J_{fw} + J_{fd} {R_n}^2} \right)$$
$$+ J_{fd} \left((R_n \omega_{1,f})^2 - (R_{prev} \omega_{1,i})^2 \right) = 0$$
$$\omega_{1,f}{}^2 \left(\eta_{pgs,n} J_{fw} + J_{fd} {R_n}^2 \right) = \omega_{1,i}{}^2 \left(\eta_{pgs,n} J_{fw} + J_{fd} {R_{prev}}^2 - (R_{prev} - R_n)^2 \left(\frac{\eta_{pgs,n} J_{fw} J_{fd}}{\eta_{pgs,n} J_{fw} + J_{fd} {R_n}^2} \right) \right)$$
$$\omega_{1,f}{}^2 \left(\eta_{pgs,n} J_{fw} + J_{fd} {R_n}^2 \right)^2 = \omega_{1,i}{}^2 \left(\eta_{pgs,n} J_{fw} + J_{fd} R_n R_{n-1} \right)^2$$

vi) $$\left(\frac{\omega_{1,f}}{\omega_{1,i}} \right)_{dis} = \frac{R_n^* R_{n-1}^* + \eta_{pgs,n}}{(R_n^*)^2 + \eta_{pgs,n}}$$, where $R_n^* = R_n \sqrt{J_{fd} / J_{fw}}$, as shown in Table 3

References

1. Metz, B., et al., *Contribution of Working Group III to the Fourth Assessment Report of the Intergovernmental Panel on Climate Change*. 2007, Cambridge, UK: Cambridge University Press.
2. Stern, N., *Stern review on the economics of climate change*. 2006, Cambridge, UK: Cambridge University Press.
3. *Energy Technology Perspectives 2008*, OECD/IEA: Paris. p. 424-447.
4. Christen, T. and M.W. Carlen, *Theory of Ragone plots.* Journal of Power Sources, 2000. **91**(2): p. 210-216.
5. Stewart, S.G., V. Srinivasan, and J. Newman, *Modeling the performance of lithium-ion batteries and capacitors during hybrid-electric-vehicle operation.* Journal of The Electrochemical Society, 2008. **155**(9): p. A664-A671.
6. Ceraolo, M., et al., *Comparison of SC and high-power batteries for use in hybrid vehicles*. 2009, SAE Technical Paper.
7. Shah, S., *The design and development of a high speed composite flywheel for hybrid vehicles. PhD Thesis*, in *Department of Mechanical Engineering, Imperial College London*. 2006.
8. Hayes, R.J., et al., *Design and Testing of a Flywheel Battery for a Transit Bus*, in *International Congress & Exposition*. 1999, SAE International: Detroit, MI, USA.
9. Flynn, M.M., J.J. Zierer, and R.C. Thompson, *Performance Testing of a Vehicular Flywheel Energy System*, in *SAE 2005 World Congress & Exhibition*. 2005, SAE International: Detroit, MI, USA.
10. Cross, D. and C. Brockbank, *Mechanical Hybrid system comprising a flywheel and CVT for Motorsport & mainstream Automotive applications*, in *SAE World Congress & Exhibition*. 2009, SAE International: Detroit, MI, USA.
11. Henning, U., et al., *Ultra low emission traction drive system for hybrid light rail vehicles*, in *International Symposium on Power Electronics, Electrical Drives, Automation and Motion.* 2006. p. 1068-1072.
12. Fuchs, R., et al., *The Making of The Full Toroidal Variator.* JTEKT Engineering Journal, English Edition, 2009(No.1006E): p. 31-36.
13. van der Sluis, F., et al., *Efficiency Optimization of the Pushbelt CVT*, in *SAE World Congress & Exhibition*. 2007, SAE International: Detroit, MI, USA.

14. Brockbank, C. *Development of full-toroidal traction drives in flywheel based mechanical hybrids*. in *Proceedings of the CVT Hybrid International Conference (CVT'10)*. 2010. Maastricht, The Netherlands.
15. Brockbank, C. and W. Body, *Flywheel-based mechanical hybrid system: simulation of the fuel consumption benefits of various transmission arrangements and control strategies*, in *ASME 2010 International Design Engineering Technical Conferences & Computers & Information in Engineering Conference*. 2010: Montreal, Canada.
16. Bottiglione, F., et al., *Mechanical Hybrid KERS Based on Toroidal Traction Drives: An Example of Smart Tribological Design to Improve Terrestrial Vehicle Performance.* Advances in Tribology. **2013**: p. 9.
17. Beachley, N.H., C. Anscomb, and C.R. Burrows, *Evaluation of split-path extended range continuously-variable transmissions for automotive applications.* Journal of the Franklin Institute, 1984. **317**(4): p. 235-262.
18. White, G., *Properties of Differential Transmissions.* The Engineer, 1967. **224**(105).
19. White, G., *Multiple-stage, split-power transmissions.* Journal of Mechanisms, 1970. **5**(4): p. 505-520.
20. Mangialardi, L. and G. Mantriota, *Power flows and efficiency in infinitely variable transmissions.* Mechanism and Machine Theory, 1999. **34**(7): p. 973-994.
21. Mantriota, G., *Power split continuously variable transmission systems with high efficiency.* Proceedings of the Institution of Mechanical Engineers. Part D: Journal of Automobile Engineering, 2001. **215**(3): p. 357-358.
22. Mantriota, G., *Performances of a series infinitely variable transmission with type I power flow.* Mechanism and Machine Theory, 2002. **37**(6): p. 579-597.
23. Mantriota, G., *Performances of a parallel infinitely variable transmissions with a type II power flow.* Mechanism and Machine Theory, 2002. **37**(6): p. 555-578.
24. Yan, H.-S. and L.-C. Hsieh, *Maximum mechanical efficiency of infinitely variable transmissions.* Mechanism and Machine Theory, 1994. **29**(5): p. 777-784.
25. Bottiglione, F. and G. Mantriota, *Reversibility of Power-Split Transmissions.* Journal of Mechanical Design. **133**(8): p. 084503-084503.
26. Beachley, N.H., et al., *Continuously-variable transmission designs for flywheel hybrid automobiles*, in *Proceedings of the lnternational Symposium on Gearing & Power Transmissions*. 1981: Tokyo. p. 393-398.
27. Martinez-Gonzalez, P., *A study on the integration of a high-speed flywheel as an energy storage device in hybrid vehicles. PhD Thesis*, in *Department of Mechanical Engineering, Imperial College London*. 2010.
28. Bottiglione, F. and G. Mantriota, *Effect of the Ratio Spread of CVU in Automotive Kinetic Energy Recovery Systems.* Journal of Mechanical Design. **135**(6): p. 061001-061001.
29. Frank, A.A., N.H. Beachley, and T.C. Hausenbauer, *The fuel efficiency potential of a flywheel hybrid vehicle for urban driving*, in *11th Intersociety Energy Conversion Engineering Conference*. 1976, American Institute of Chemical Engineers: State Line, Nev. p. 17-24.
30. Barr, A. and A. Veshagh, *Fuel economy and performance comparison of alternative mechanical hybrid powertrain configurations*. 2008, SAE Technical Paper.
31. van Berkel, K., et al., *Fast and Smooth Clutch Engagement Control for a Mechanical Hybrid Powertrain.* Control Systems Technology, IEEE Transactions on, 2014. **22**(4): p. 1241-1254.
32. Diego-Ayala, U., et al., *The mechanical hybrid vehicle: an investigation of a flywheel-based vehicular regenerative energy capture system.* Proc IMechE, Part D: Journal of Automobile Engineering, 2008. **222**(11): p. 2087-2101.
33. Guzzella, L. and A. Sciarretta, *Vehicle Propulsion Systems: Introduction to Modeling and Optimization*. 3rd ed. 2013, Berlin: Springer.

34. Fritzson, P. and P. Bunus. *Modelica - a general object-oriented language for continuous and discrete-event system modelling and simulation*. in *Proceedings of the 35th IEEE annual simulation symposium*. 2002.
35. Fritzson, P., et al. *OpenModelica - A free open-source environment for system modeling, simulation, and teaching*. in *IEEE International Symposium on Computer-Aided Control Systems Design, 2006*. 2006. Munich, Germany: IEEE.
36. van Berkel, K., et al., *Optimal Control of a Mechanical Hybrid Powertrain.* Vehicular Technology, IEEE Transactions on, 2012. **61**(2): p. 485-497.
37. van Berkel, K., et al., *From Optimal to Real-Time Control of a Mechanical Hybrid Powertrain.* Control Systems Technology, IEEE Transactions on, 2014. **PP**(99): p. 1-1.
38. White, G., *Compounded two-path variable ratio transmissions with coaxial gear trains.* Mechanism and Machine Theory, 1976. **11**(3): p. 227-240.
39. Naunheimer, H., et al., *Automotive Transmissions: Fundamentals, Selection, Design and Application*. 2nd ed. 2011, Berlin: Springer.